Growth, structure, electronic, and magnetic properties of MgO/Fe(001) bilayers and Fe/MgO/Fe(001) trilayers

M. Klaua, D. Ullmann, J. Barthel, W. Wulfhekel, and J. Kirschner
Max-Planck-Institut für Mikrostrukturphysik, Weinberg 2, 06120 Halle, Germany

R. Urban, T. L. Monchesky, A. Enders, J. F. Cochran, and B. Heinrich
Department of Physics, Simon Fraser University, Burnaby, British Columbia, Canada V5A 1S6
(Received 5 February 2001; published 11 September 2001)

Single-crystal epitaxial MgO thin films were grown directly onto high-quality Fe single crystal and Fe whisker substrates and covered with Fe/Au layers. Reflection high-energy electron diffraction and low-energy electron diffraction patterns and scanning tunneling microscopy images showed that the growth of MgO proceeded pseudomorphically in a nearly layer-by-layer mode up to six monolayers. A misfit dislocation network is formed for MgO layers thicker than six monolayers. The thin MgO films were characterized electrically by scanning tunneling spectroscopy. The tunneling barrier in MgO was found to depend on the MgO layer thickness, starting from 2.5 eV at two monolayer thickness to the expected full barrier of MgO of 3.6 eV at six monolayers. A small fraction of the scanned area showed randomly placed spikes in the tunneling conductance. Tunneling *I-V* curves at the defects showed a lower tunneling barrier than that in the majority of the MgO film. The total tunneling current integrated over areas of 100×100 nm^2, however, was not dominated by spikes of higher conductance. These local defects in the MgO barrier were neither related to atomic steps on the Fe substrates nor to individual misfit dislocations. Magnetic anisotropies and exchange coupling in Fe/MgO(001) and Fe/MgO/Fe(001) structures were studied using ferromagnetic resonance and Brillouin light scattering.

DOI: 10.1103/PhysRevB.64.134411 PACS number(s): 68.55.−a, 73.40.Gk, 73.40.Rw, 85.30.Mn

I. INTRODUCTION

Studies of spin-dependent tunneling in structures consisting of two metallic ferromagnetic (FM) films separated by an insulating spacer are currently of high interest in the research field of magnetic nanostructures. Magnetic tunnel junctions (MTJ's) play a significant role in the development of nonvolatile magnetic random access memories (MRAM's). The MTJ's used so far mostly rely on amorphous Al_2O_3 oxide as the insulating barrier. The electron tunneling in such amorphous barriers is complex; it consists of random hopping between oxide resonant states which are created by a number of poorly understood defects. The lateral component of the electron momentum, $k_\parallel$, is randomized by scattering in the barrier, such that the tunneling current is not only determined by the intrinsic band structrure of the electrons and the oxide barrier but is significantly affected by lattice disorder in the barrier. The total randomization of $k_\parallel$ results in averaging of the tunnel magnetoresistance (TMR) over the Fermi surface of the *s* and *p* valence electrons.[1] As a result of this, spin-dependent tunneling through amorphous barriers has successfully been described by only one parameter: the effective spin polarization of the ferromagnetic films.[2] The recent theoretical calculations of intrinsic electron tunneling transport by the Landauer formalism using fully spin-dependent electron band structure provide challenging predictions. The tunneling conductance in Fe/MgO/Fe(001) is governed by the majority spin electrons. The tunneling resistance for the parallel orientation of the magnetic moments is estimated to be 100 times smaller than that for the antiparallel orientation of the magnetic moments[3] due to the absence of scattering in the barrier.

In this paper we show that one is able to grow nearly perfect crystalline MgO(001) films on high-quality single crystals of Fe. The *I-V* characteristics of these structures are dominated by the intrinsic properties of the Fe/MgO/Fe(001) structure, allowing one, in principle, to test the wealth of predictions based on first-principles calculations. This paper will be limited to the structural, magnetic, and electron transport studies in zero applied field only. Our present scanning tunneling microscopy (STM) system did not allow us, up to now, to investigate magnetoresistance, i.e., tunneling conductance as a function of an applied field.

II. SUBSTRATE PREPARATION, GROWTH OF MgO, AND Fe FILMS

For the extensive study of the growth of MgO on Fe(001) and of Fe/MgO/Fe(001) trilayers two different types of Fe substrate crystals were used: Fe(001) whiskers and single-crystal Fe(001) disks. Fe whiskers were prepared by chemical vapor transport using the reduction of $FeCl_2$ in a H_2 atmosphere. The whiskers are long rectangular bars with {001} facets. The whiskers are usually 3–10 mm long and 100–300 μm wide. Fe(001) crystal disks of 10 mm diameter and 3 mm thickness were oriented using x-ray diffraction and mechanically polished with less than 0.2° deviation from the (001) plane and annealed at 1170 K in H_2 for 14 days. The final preparation of Fe whiskers and disk substrates was carried out in UHV using 2 kV Ar ion bombardment first at 300 K and then subsequently at 500 K for 3 h in order to remove interstitial carbon. The substrates were brought rapidly to 870 K, and sputtering was switched off after 5 min. A 6 min annealing at 870 K (without sputtering)

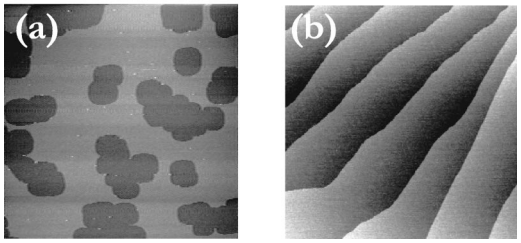

FIG. 1. STM topographical images: (a) Clean Fe(001) whisker (tunneling conditions: +0.6 V, 0.6 nA, 2000×2000 nm^2). (b) Clean Fe(001) bulk crystal (tunneling conditions: +0.54 V, 0.66 nA, 500×500 nm^2).

was followed by final rapid cooling to 300 K. Auger electron spectroscopy (AES) analysis revealed less than 1% of C and N impurities on the surface. Low-energy electron diffraction (LEED) and reflection high-energy electron diffraction (RHEED) patterns showed very sharp spots (see below). Figure 1(a) shows the STM image of an Fe(001) whisker after preparation in UHV. The dark regions are monoatomic extended holes ($1-2$ μm wide) in an otherwise flat and step-free surface. Figure 1(b) is a typical STM image of an Fe(001) disk sample showing atomic steps with a mean separation of 100 nm. This corresponds to $<0.1°$ deviation from a (001) surface plane.

MgO layers were deposited at 295 K using electron beam evaporation from a 3-mm-diam MgO rod of 99.8% purity. Results of a comparative study using pulsed laser deposition (PLD) of MgO will be presented elsewhere.[4] The background pressure of low 10^{-10} mbar rose to a value high in the 10^{-10} mbar range during deposition. The growth mode was monitored *in situ* using RHEED intensity measurements. The surface crystallography and the epitaxial growth mechanism were further characterized by means of LEED. The purity and stoichiometry of the MgO grown on Fe was checked with AES and ultraviolet photoemission spectroscopy (UPS). The MgO Auger line shapes were consistent with those listed for magnesium monoxide,[5] indicating the correct stoichiometry. No impurities were found within the sensitivity of our AES setup. UPS spectra of five monolayer (5 ML) MgO on Fe revealed an energy difference of 4.2 eV between the upper Mg 1*s* and O 2*p* valence-band edge and the Fermi level of Fe. Taking the band gap of MgO as 7.8 eV,[6] this results in a tunneling barrier height of 3.6 eV for electrons at the Fermi energy of Fe tunneling through the MgO. The surface topography of the MgO films was studied using STM. Scanning tunneling spectroscopy (STS) was applied to characterize the electron transport through the MgO films.

The top Fe layer was deposited at 295 K either by means of a thermal source at a growth rate of about (1 ML)/min or by means of PLD (248 nm wavelength, 30 ns pulses). The samples were protected in ambient by a 20-ML-thick Au(001) capping layer.

III. STRUCTURE AND DEFECTS OF MgO ON Fe(001)

The growth of MgO was monitored by means of RHEED. The inset of Fig. 2(a) shows the RHEED pattern for an inci-

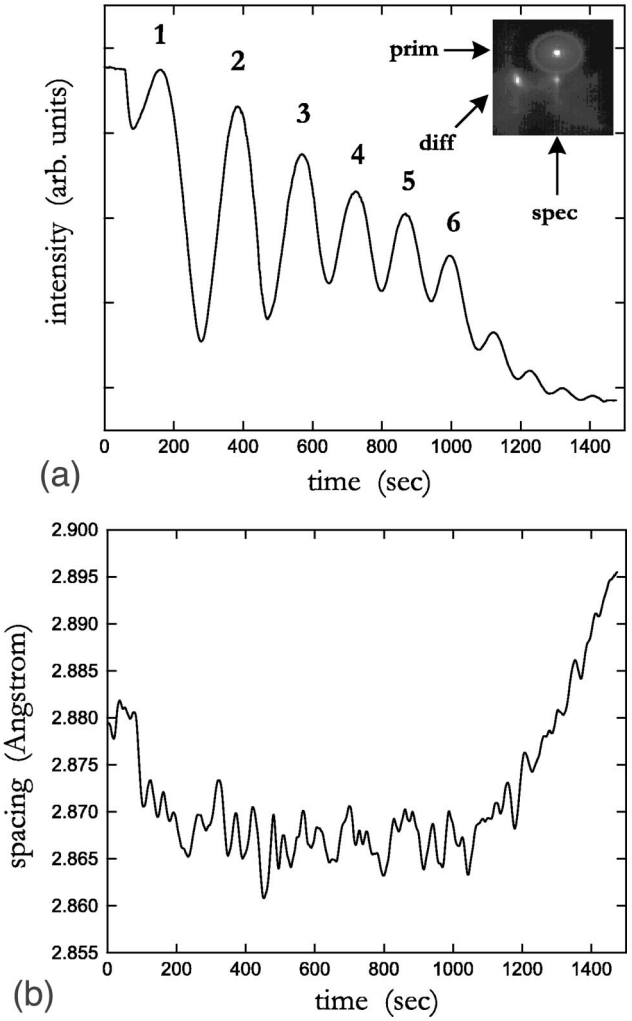

FIG. 2. (a) RHEED diffracted beam intensity oscillations vs time for deposition of MgO on Fe(001). Inset shows the RHEED pattern before deposition. (b) Measured lateral spacing of grown MgO layers.

dence angle of $0.7°-0.8°$ (first anti-Bragg condition) and an azimuthal direction near the [100] Fe axis. The Fe crystal was rotated by 1.5° from the exact [100] in-plane crystallographic direction in order to make the line connecting the specular and diffracted beams parallel to the shadow edge. Under these conditions strong RHEED intensity oscillations were found [see Fig. 2(a)] and the intensities of the diffracted and the specular (not shown) beams were oscillating nearly out of phase. The intensity maxima of the diffracted beam correspond to the best surface filling of the MgO films as has been checked with STM (see below). RHEED oscillations are a strong indication of a layer-by-layer growth of MgO on Fe(001) which is thermodynamically favored because of the low surface energy of MgO (1.16 J/m^2) (Ref. 7) in comparison to that of Fe (2.9 J/m^2).[8] The intensity drops dramatically after the sixth ML of MgO. This is correlated with an observed increase in the lateral spacing of the MgO lattice, as depicted in Fig. 2(b). The lateral lattice spacing was determined from the measurement of the peak intensity profiles through the specular and diffracted beams. MgO grows

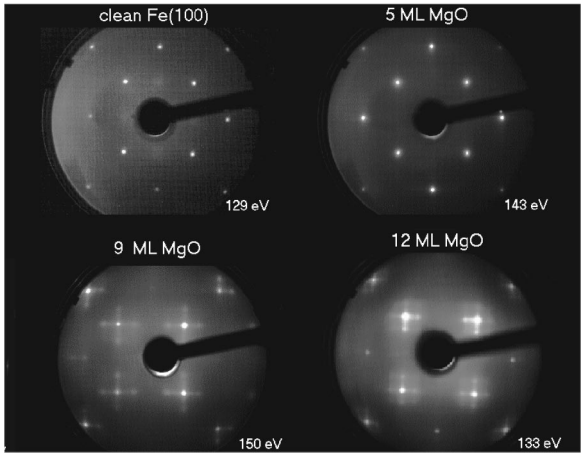

FIG. 3. LEED patterns for a clean Fe(001) whisker and after deposition of 5 ML, 9 ML, and 12 ML of MgO. The LEED patterns were taken at energies as indicated.

pseudomorphically on Fe(001) up to 6 ML with an epitaxial relationship Fe(001)[110]//MgO(001)[100] and a 3.8% compression of the MgO lattice.[9,10] After 6 ML a partial lattice relaxation sets in, resulting in an increased lateral lattice spacing. The resulting misfit dislocation network near the Fe/MgO interface leads to increased surface roughness and by this to a reduction of the RHEED intensities.

The most convincing indication of the pseudomorphic growth and the subsequent sharp onset of misfit dislocations can be seen in the LEED patterns (Fig. 3). The LEED spots are very sharp on a clean bcc Fe(001) whisker, indicating a superb surface quality. Similar sharp spots from the MgO(001) surface were observed after growth of up to 6 ML MgO. For thicknesses greater than 7 ML of MgO the LEED patterns showed four additional satellite spots around each main MgO diffraction spot. The four lines connecting any given set of satellite spots and their central diffraction spot are directed along equivalent $\langle 100 \rangle$ in-plane crystallographic directions of the MgO lattice. The splitting between the satellite and main diffraction spots decreases with increasing thickness of MgO; see Fig. 3. The LEED patterns show that the splitting increases proportionally with the electron beam energy. This behavior can be explained by a model which includes edge dislocation formation[10] at the Fe/MgO interface. The MgO lattice warps in a narrow region above the misfit dislocation lines. The warped surface creates tilted reciprocal-space rods which satisfy the fourfold in-plane symmetry of the Fe(001) template. The LEED satellite spots are caused by the tilted reciprocal rods due to the network of dislocation lines. The effective tilt angle is 3.5° for 7 ML and decreases to 1.5° for 15 ML thick MgO films.[11]

The characterization of morphology and crystallography by RHEED and LEED could reveal only spatially averaged information. Direct imaging using *in situ* STM is needed to obtain more detailed information about the growth mode of the MgO films. STM imaging of ultrathin insulator films requires a proper choice of bias voltage. To obtain a topographic image of the MgO surface one needs to establish tunneling from the occupied states of the STM tip into the conduction band of MgO. The bulk band gap of MgO is 7.8 eV. Assuming that the Fermi level of MgO lies somewhere in the midgap one would expect that the bias voltage should be close to $+3.9$ V in agreement with our UPS results.

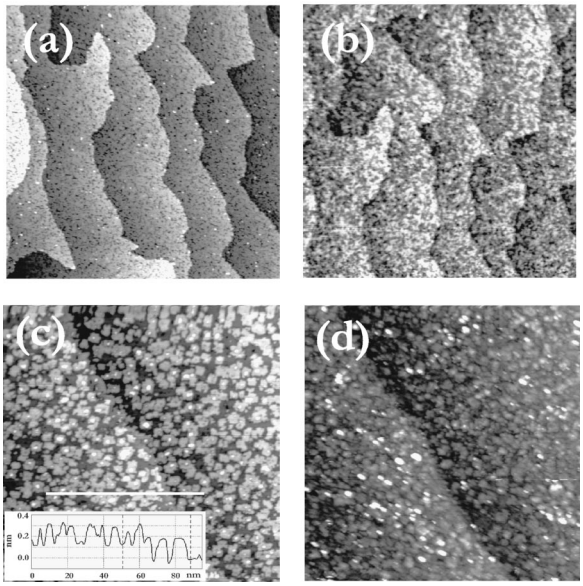

FIG. 4. STM topographic imaging of MgO layers on Fe(001) in dependence on bias voltages. (a) 1.9 ML MgO, rms roughness: 0.063 nm ($+3$ V, 0.66 nA, 300×300 nm^2). (b) 1.9 ML MgO ($+4$ V, 0.66 nA, 300×300 nm^2). (c) 3.6 ML MgO, rms roughness: 0.074 nm ($+4$ V, 0.8 nA, 150×150 nm^2). Inset shows plot of topographical height vs position along a horizontal line. (d) 3.6 ML MgO ($+2$ V, 0.3 nA, 150×150 nm^2).

In Fig. 4, STM topographic images of MgO layers of 1.9 ML and 3.6 ML thickness are shown as a function of the bias voltage. A nearly completely filled second atomic layer of MgO in Fig. 4(a) was obtained by stopping the MgO deposition at the second maximum of the diffracted RHEED beam intensity (see Fig. 2). The thickness of 3.6 ML in Fig. 4(c) was obtained by stopping the deposition at the minimum of the RHEED oscillations following the third maximum (see Fig. 2). Figure 4(a) was taken with $+3$ V sample bias voltage. It gives a clear topographic image of a nearly perfect two-dimensional growth of MgO on Fe(001) with clearly visible atomic steps of the Fe template. The rms roughness of this mainly two atomic level growth amounts to 0.063 nm. The gray level corresponds to 2 ML of MgO, the black contrast are holes of 1-ML-thick MgO, and finally the white spots correspond to small islands of 3 ML of MgO. Hence, also STM shows that MgO grows in a nearly perfect layer-by-layer mode as already concluded from the RHEED oscillations. The STM image in Fig. 4(b) was taken with the higher sample bias of $+4$ V. This results in a more complex image with some additional features whose origin is not known yet. The STM image, Fig. 4(c), for a sample of 3.6 ML thickness using a bias voltage of $+4$ V gives again a clear topographic contrast. In this case the MgO surface consists mainly of two atomic layers. The dark areas correspond to the third ML. The brighter islands correspond to the fourth atomic layer and are of square shape. Some small speckles of the fifth ML (white spots) are also present. The inset shows a height profile along a horizontal line across the substrate

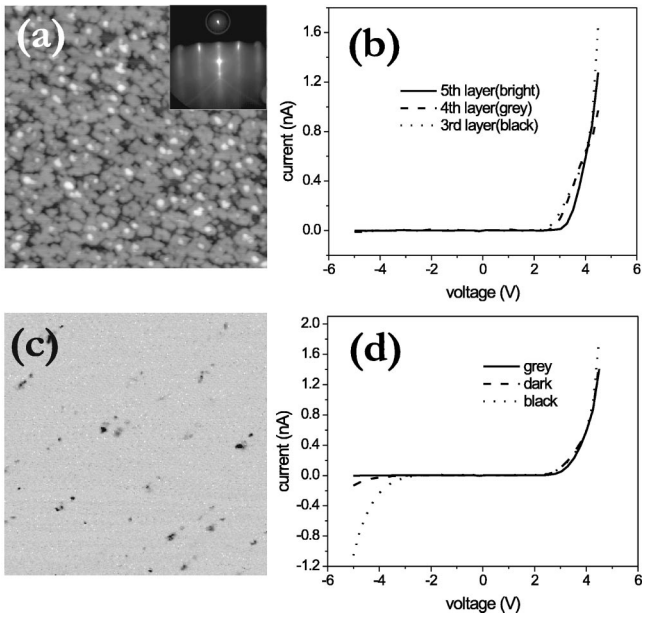

FIG. 5. (a) Morphology of 3.8 ML MgO on Fe(001), rms roughness: 0.075 nm (+4.1 V, 0.66 nA, 100×100 nm^2). The inset shows a RHEED pattern along a [110] crystallographic direction of MgO. (b) Tunneling spectra for different thicknesses of MgO shown in (a). (c) Spectroscopic current image of local defects taken at a bias voltage of −4 V (100×100 nm^2). (d) Tunneling spectra of a defect free area (gray) and of different local defects (dark and black).

step. The height difference between the minima of the profile in the left side and the minima of the right side amounts to 0.14 nm which is the height of an Fe(001) atomic step. The height of the two-dimensional islands is 0.2 nm which corresponds to an MgO atomic step. As expected, under optimal conditions for topographic imaging one obtains the correct heights for MgO islands and Fe(100) atomic steps. In Fig. 4(d) at a lower bias voltage of +2 V which is within the MgO band gap the electrons tunnel directly from the tip to the conducting substrate and the oxide layer acts only to modulate the potential barrier as a function of position. Therefore the additional contrast in Fig. 4(d) may be related to inhomogeneities in the substrate-oxide interface.[12] The above results show that optimal conditions for STM imaging are fulfilled for positive-bias voltages which are close to half of the MgO band gap energy. There is only a weak dependence of the optimal conditions on the film thickness (see below).

The relationship between the MgO layer thickness and electron transport through the MgO layers was obtained by taking STM topographic images and acquiring tunneling *I-V* curves simultaneously. Local *I-V* curves in every point and spectroscopic current images at any applied scan voltage could be displayed afterwards. The total recording time was 10–20 min per image. Figure 5(a) shows the topographic image of a 3.8 ML MgO film grown on Fe(001). Three contrast levels correspond to the complete third layer (black), the incomplete fourth layer (gray), and some islands of the fifth layer (bright), indicating a nearly ideal layer-by-layer growth. Averaged *I-V* tunneling spectra for potentials ranging from +4.5 V to −4.5 V are shown for each exposed atomic layer in Fig. 5(b). The curves exhibit a strongly pronounced current asymmetry. The increase of the tunneling current for potentials greater than +2.5 V indicates tunneling from the Fermi edge of the PtIr tip into the conduction band of MgO. On the other hand, tunneling from the MgO valence band for negative potentials is negligible. Such observed tunneling asymmetry is expected for a perfect insulator.

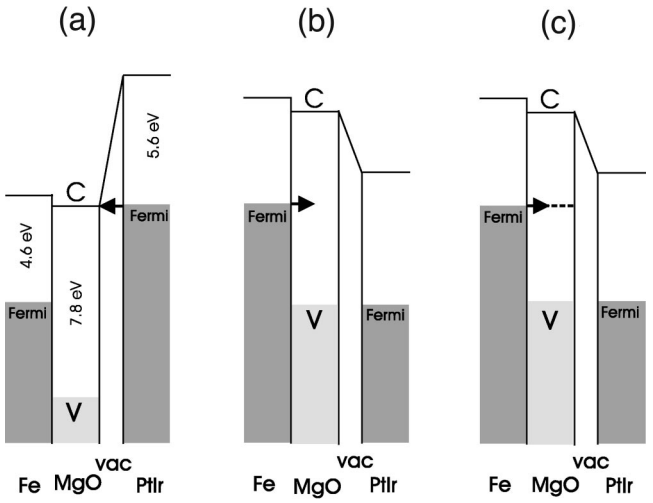

FIG. 6. A sketch of energy bands of the Fe/MgO/vacuum/PtIr tip structure. (a) Bias voltage +4 V, tunneling into the conduction band of MgO through the vacuum barrier. (b) Bias voltage −4 V, tunneling from the valence band of MgO through the vacuum barrier. (c) Negative-bias voltage, tunneling through additional defect states midway between the valence and conduction bands of MgO.

In Fig. 6 sketches of energy diagrams of the Fe(001)/MgO/vacuum/PtIr tip structure for different biases are shown with a work function of 4.6 eV for the Fe(001) substrate, a band gap of 7.8 eV for the MgO barrier, and a work function of 5.6 eV for the PtIr tip, respectively. In Fig. 6(a) applying a positive bias voltage of +4 V results in tunneling from the filled states of the tip through the vacuum barrier and the conduction band of MgO into empty states of the Fe substrate. On the other hand, in Fig. 6(b) a negative bias of −4 V applied does not give rise to a noticeable tunneling from the Fe substrate through the MgO barrier and the vacuum barrier. Tunneling from the Fermi energy of the Fe substrate is suppressed by the large thickness of the effective barrier and tunneling from the valence band of MgO is suppressed due to the large active barrier height of over 7 eV. But if defect states exist within the band gap of MgO, as in Fig. 6(c), then the tunneling probability via these defect states is largely enhanced.

The *I-V* characteristics in Fig. 5(b) give no hint of the presence of any defects in the MgO layer. At negative voltages, we found a vanishing tunneling current in the spectra in agreement with the previous considerations. At positive voltages, the tunneling current sets in around +3 V when the energy of the tunneling electrons approaches the conduction band of MgO. The spectroscopic current image at −4 V in Fig. 5(c), however, shows some localized regions (black

spots) of increased tunneling current from the Fe substrate through the MgO barrier into the tip. Most of the scanned area shows a gray contrast with *I-V* curves corresponding to a perfect insulating barrier. The averaged spectrum for these regions is shown as the asymmetric solid curve in Fig. 5(d). The local darker spots in Fig. 5(c) correspond to the dashed curve in Fig. 5(d) and exhibit an enhanced tunneling current for a potential beyond -3 V. Finally, the black spots in Fig. 5(c) correspond to the dotted curve in Fig. 5(d) with an observable tunneling current starting already at -2.5 V. The local defects have dimensions of a few nm. They are not correlated with the surface topography, as one can conclude from comparing Figs. 5(a) and 5(c). The tunneling from the Fe substrate through the valence band of MgO requires a sufficient negative bias to overcome the MgO barrier and the vacuum barrier [see Fig. 6(b)], leading to a strong asymmetry in the tunneling current. The *I-V* curves for a positive bias on the defect regions in Fig. 5(d) are nearly identical to those measured on the good regions of the sample. However, there is a noticeable rise in tunneling current for the defects for negative bias; see Fig. 5(d). This means that the defects have additional energy levels inside the MgO band gap that allow a noticeable tunneling current for negative bias; see Fig. 6(c). Since the increase in tunneling current in defects occurs at negative voltages which are close in their absolute value to the positive potential $+2.5$ V (allowing tunneling into the conduction-band edge of the MgO film), it is reasonable to assume that the defect energy levels in the MgO gap are midway between the valence and conduction bands. The origin of these defects is not yet known. They are most likely caused by structural defects, which create localized resonant tunneling states in the MgO band gap.[13]

Surprisingly, no defectlike curves were found in local *I-V* curves near the positions of misfit dislocation lines. The defect analyses using STM and STS were carried out for a 7-ML-thick MgO film. The RHEED and LEED pattern analyses showed the presence of edge misfit dislocations. The topographic image of Fig. 7(a) shows several features: (i) three-level contrast of the growing MgO film, (ii) an area corresponding to an atomic step in the Fe substrate [see the upper right corner of Fig. 7(a)], and (iii) narrow ribbonlike lines (see arrows) which cross each other at right angles. These lines outline the warped regions of the surface along the buried misfit dislocations. Along a misfit dislocation line which is assumed to be incorporated near the substrate-oxide interface the MgO lattice shows a displacement field which produces a surface step as well as a *s*-like tilting along the MgO surface.[14] STM detects the sloped regions along the buried dislocations as ribbonlike lines and allows one to determine their width (about 3 nm) and the mean dislocation separation (about 30 nm). The measured separation and the width are in agreement with model calculations.[14] The tunneling spectra in Fig. 7(b) from different thickness levels show essentially the same behavior as those in Fig. 5(b). The spectroscopic current image for -8 V in Fig. 7(d) reveals again localized defect regions with tunneling spectra analogous to those shown in Fig. 5(d). The most interesting point to stress here is that the defects shown in Fig. 7(c) are correlated neither with the substrate step of the MgO/Fe(001)

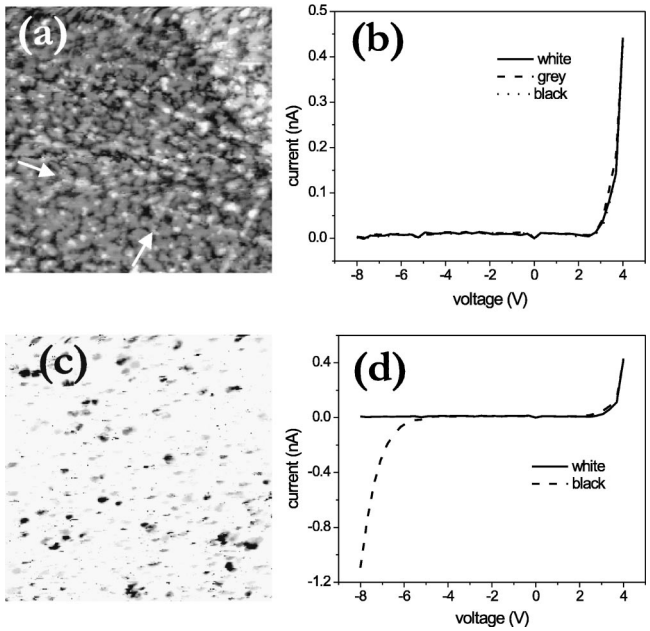

FIG. 7. (a) Morphology of 7 ML MgO on Fe(001) exhibiting dislocation traces (arrows), rms roughness: 0.092 nm ($+4$ V, 0.29 nA, 100×100 nm^2). (b) Tunneling spectra for different thicknesses of MgO shown in (a). (c) Spectroscopic current image of local defects at a bias of 8 V(100×100 nm^2). (d) Tunneling spectra from defect free areas (solid) and from local defects (dashed) shown in (c).

interface nor with the dislocation lines in the MgO film. Therefore we assume that the observed defects are intrinsic to the MgO layer due to the agglomeration of atomic defects, the nature of which is not yet known. The preparation of MgO tunnel barriers does not have to be restricted to a thickness of pseudomorphic growth, i.e., thickness less than 6 ML, but can be carried out for thicker MgO films without encountering degradation of their tunneling properties.

The rapid onset of the tunneling current from the PtIr tip into the conduction band of MgO for positive bias was used to determine the thickness dependence of the tunneling barrier height for positive biases [see Fig. 5(b)]. The barrier height was taken as that voltage for which tunneling currents of 0.01 nA were observed. In Fig. 8 the measured barrier height is plotted half logarithmically versus the MgO thickness. These experimentally measured barrier heights show a continuous increase with thickness starting with 2.5 eV at 2 ML to the full 3.6 eV barrier at 6 ML coverage. Assuming that the Fermi level lies in the midgap, then the band gap is twice the height of the measured barrier. Thus the band gap in MgO films seems to be thickness dependent. The band gap increases from 5.0 to 7.6 eV as the MgO film thickness varies from 2 to 6 ML. The increase of the barrier height can be interpreted as a size effect not yet addressed theoretically to our knowledge. But there is another contribution to the thickness dependence in our special case. Using the same Fe(001) crystal and MgO evaporator under similar deposition conditions it was shown by a glancing x-ray diffraction study that a substoichiometric epitaxial FeO layer is formed at the Fe/MgO interface.[15] Because of the lower band gap of 2.4 eV of

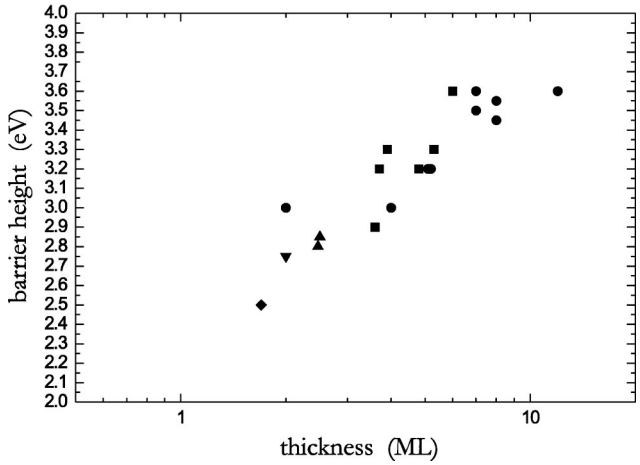

FIG. 8. Measured barrier height vs thickness of MgO for slightly different positive-bias voltages. The symbols correspond to the following biases: □ (+4.09 V), ○ (+4.01 V), △ (+3.55 V), ▽ (+3.21 V), and ◇ (+3.08 V).

FeO, the measured barrier height is reduced additionally to the thickness dependence of the MgO barrier.

IV. STRUCTURE AND DEFECTS OF Fe/MgO /Fe(001) TRILAYERS

A complete tunnel junction was prepared by adding 5 ML of Fe on top of a 2 ML MgO on Fe(001) structure using PLD at 300 K. Fe grows epitaxially on MgO (Ref. 9) with the same relationship given above for MgO on Fe(100), but due to the lower surface energy of MgO (1.16 J/m^2) (Ref. 7) in comparison to that of Fe (2.9 J/m^2),[8] the growth proceeds in a typical three-dimensional pattern. PLD creates an enhanced density of nuclei, allowing one to get a continuous Fe film at the early stages of the growth in spite of the formation of three-dimensional islands which is thermodynamically favored.

The STM image of a 5-ML-thick Fe layer on 2 ML MgO on Fe(001) in Fig. 9(a) shows a high island density with an enhanced rms roughness of 0.158 nm. The RHEED pattern shown in the inset of Fig. 9(a) exhibits a clear three-dimensional-like appearance but the entire Fe layer has crystalline structure. Tunneling spectra of the complete tunnel junction in Fig. 9(b) are nearly the same as those obtained using bare MgO layers on Fe(001); compare Fig. 5(b), Fig. 7(b), and Fig. 9(b). This indicates that the thin Fe film is basically transparent for electrons that tunnel and that diffuse transport in the Fe film does not play an important role.[16] The local spectra for the tunneling structure terminated by a conducting layer of Fe show also very similar features. The small differences in the tunneling currents (white, gray, black curves) at positive bias shown in Fig. 9(b) are not correlated to the topography of the Fe capping layer in Fig. 9(a). Differences in the local tunneling were obtained again by a spectroscopic current image at −3 V; see Fig. 9(c). The majority of the area of gray contrast shows a perfect tunnel barrier of very low tunneling current which corresponds to the asymmetric solid curve in Fig. 9(d). Only randomly

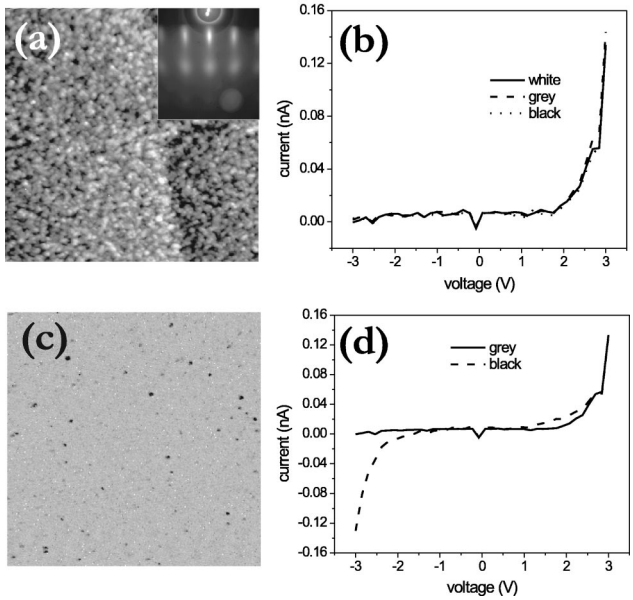

FIG. 9. (a) Morphology of the top iron surface of the trilayer tunnel junction of 5 ML Fe on 2 ML MgO on Fe(001), rms roughness: 0.158 nm (+3.0 V, 0.1 nA, 150×150 nm^2). The inset shows the RHEED pattern with primary electron beam along the [110] direction of bcc Fe. (b) Tunneling spectra for different thicknesses of Fe shown in (a). (c) Spectroscopic current image at a bias voltage of −3 V (150×150 nm^2). (d) Tunneling spectra from the defect-free areas (solid) and defect spots (dashed) shown in (c).

placed black spots in Fig. 9(c) indicate enhanced localized tunneling currents at −3 V which correspond to the dashed curve in Fig. 9(d). These black spots do not show any correlation to the topography in Fig. 9(a). This means they are related to intrinsic defects in the oxide barrier similar to those obtained from bare MgO layers in Figs. 5 and 7.

The ability to locally see different tunneling spectra on the conducting Fe top layer grown on the insulator film and the almost identical shape of the spectra in comparison to those of bare MgO films points at a high fraction of ballistic electrons. If the transport of the electrons that tunnel into the top Fe film were entirely diffusive, the tunneling spectra should resemble that of simple tunneling between two metals; i.e., they should not show the features that are characteristic for tunneling through an insulator film. In the case of diffusive transport the tunneling probability and, by this, the tunneling current would be determined only by the tunneling between the tip and the top electrode. The electrons that tunnel from the tip into the top Fe film would diffuse away and tunnel at an arbitrary position from the top Fe film through the MgO into the substrate. In this case, also no variation of the local tunneling spectrum should be observed. If, however, there is an additional ballistic channel for the electrons to cross the top Fe electrode, the properties of the MgO film underneath the tip also determine the total tunneling current. When the spectra are also determined by the second tunneling barrier through the oxide, also lateral variations of the tunneling spectra are observed due to variations in the second barrier. When the energy of the electrons is close to the local barrier height of the buried MgO film, the hot electrons reaching the

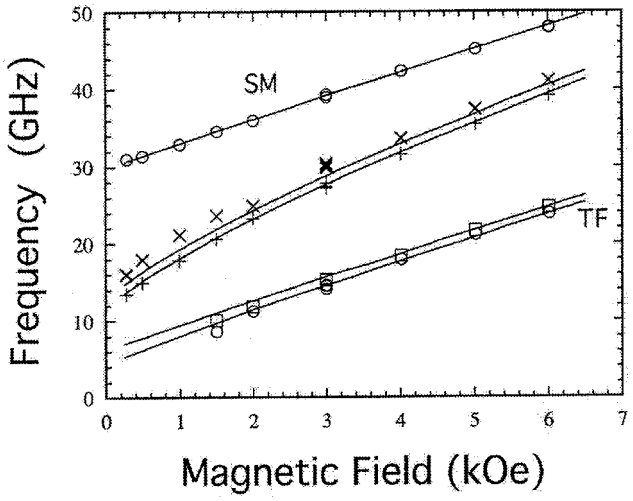

FIG. 10. Frequencies vs applied magnetic field for the composite specimen Fe-whisker/5 ML MgO/9 ML Fe/12 ML Ni/20 ML Au(001). TF, thin-film frequencies; □, upshifted frequencies; ○, downshifted frequencies. SM, bulk iron surface mode frequencies. ×, upshifted bulk iron manifold edge frequencies; + −, downshifted bulk iron manifold edge frequencies. The solid lines were calculated for zero exchange coupling using following parameters: (1) Thin film: $4\pi M_s = 13.3$ kG, $g = 2.12$, perpendicular surface anisotropy $K_s = 1.64$ erg/cm^2, in-plane anisotropy parameter $K_1 = 4.76\times10^5$ erg/cm^3, and thickness $d = 3$ nm. (2) Bulk iron: $4\pi M_s = 20.4$ kG, $g = 2.09$, exchange stiffness $A = 2.03\times10^{-6}$ erg/cm, and in-plane anisotropy parameter $K_1 = 4.76\times10^5$ erg/cm^3.

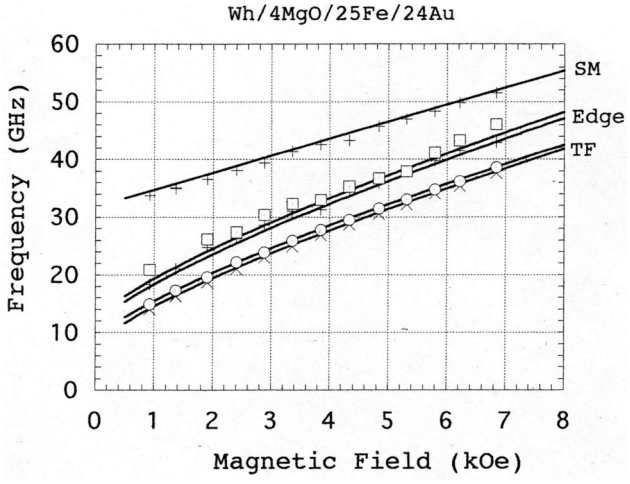

FIG. 11. Frequencies vs applied magnetic field for the composite specimen Fe-whisker/4 ML MgO/25 ML Fe/24 ML Au(001). TF, thin-film frequencies: ○, upshifted frequencies; ×, downshifted frequencies. SM, iron whisker surface mode frequencies. Edge-bulk iron manifold edge frequencies, respectively. The solid lines were calculated for zero exchange coupling using following parameters: (1) Thin film: $4\pi M_s = 21.4$ kG, $g = 2.09$, perpendicular surface anisotropy $K_s = 1.65$ erg/cm^2, in-plane anisotropy parameter $K_1 = 4.0\times10^5$ erg/cm^3, and thickness $d = 3.58$ nm. (2) Bulk iron: $4\pi M_s = 21.4$ kG, $g = 2.09$, exchange stiffness $A = 2.03\times10^{-6}$ erg/cm, perpendicular surface anisotropy $K_s = 1.0$ erg/cm^2, and in-plane anisotropy parameter $K_1 = 4.76\times10^5$ erg/cm^3.

MgO are transmitted with a relatively high probability. By this, small variations in the electronic structure of the MgO lead to strong variations in the local tunneling current. This mechanism allows the characterization of the complete MTJ's with thin top electrodes[16] and allows one in principle to study the role of defects in tunnel magnetoresistance.

V. MAGNETIC PROPERTIES

The quality of the Fe top electrode and the strength of the magnetic coupling between this electrode and the bulk whisker were assessed using Brillouin light scattering (BLS). The BLS measurements were carried out using fully crystalline Fe-whisker/5 ML MgO/9 ML Fe/12 ML Ni/20 ML Au(001) and Fe-whisker/4 ML MgO/25 ML Fe/24 ML Au(001) structures. The peaks corresponding to light scattered from the spin waves in the thin-film Fe/Ni(001) and Fe(001) electrodes were strong and narrow; the frequency width was due to the instrumental resolution, approximately 1 GHz. This suggests that the Fe/Ni and Fe electrodes were either weakly coupled or uncoupled to the bulk whisker substrate. The dependence of the spin-wave frequency on applied magnetic field was fitted using micromagnetic calculations for the magnetic thin-film structures grown on bulk substrates.[17] The measured BLS data can be fitted very well (see Fig. 10) using zero coupling to the whisker substrate, $4\pi M_s = 13.3$ kG, the spectroscopic splitting factor $g = 2.12$, and the perpendicular uniaxial anisotropy parameter $K_s = 1.64$ ergs/cm^2 with the easy axis perpendicular to the film surface, in-plane anisotropy parameter $K_1 = 4.76\times10^5$ ergs/cm^3, and the Fe film thickness $d = 3$ nm for the Fe-whisker/5 ML MgO/9 ML Fe/12 ML Ni/20 ML Au(001) sample. The value $g = 2.12$ was calculated for the composite Fe/Ni(001) film using the scaling calculation described by Heinrich *et al.*[18] The scaling calculations yielded $4\pi M_s = 16.5$ kG, a value somewhat larger than that required by the BLS data. The surface uniaxial anisotropy K_s was obtained from our ferromagnetic resonance (FMR) studies using Fe(001) films grown on single-crystal MgO(001) substrates and covered by Au(001). The uniaxial perpendicular anisotropy was found to be inversely proportional to the Fe film thickness, indicating that the uniaxial anisotropy originates at the interfaces.[19] The thin-film BLS frequencies depend upon the in-plane magnetocrystalline anisotropies through an effective field $2K_1/M_s$. For the Fe/Ni film we used $K_1 = 4.76\times10^5$ ergs/cm^3, the value for bulk iron, for lack of data on the in-plane anisotropy for our Fe/Ni(001) film. This uncertainty results in an uncertainty of the order 0.5 kG in the thin-film magnetization.

The BLS resonant spectra for the Fe-whisker/4 ML MgO/25 ML Fe/24 ML Au(001) sample (see Fig. 11) were well fit using the following parameters: a negligible exchange coupling between the Fe film and Fe whisker, $K_s = 1.65$ ergs/cm^2 for the Fe film (determined from FMR), a fourfold in-plane anisotropy (determined from FMR) nearly equal to that of bulk Fe, $K_1 = 4\times10^5$ ergs/cm^3, and a uniaxial anisotropy $K_s = 1.0$ ergs/cm^2 for the Fe whisker/MgO interface. The total uniaxial anisotropy for the Fe film is given by the sum of the Fe/MgO(001) and Fe/Au(001)

interface anisotropies. The interface anisotropy for the Fe/Au(001) interface is 0.47 ergs/cm^2.[19] Therefore the interface anisotropy for the Fe/MgO(001) interface is $1.64-0.47=1.18$ ergs/cm^2. The interface anisotropy at the Fe/MgO interface is large compared to metallic interfaces. The interface anisotropies for Fe/Au (0.47 ergs/cm^2), Fe/Ag (0.81), Fe/Pd (0.17), Fe/Cr (0.5), and Fe/Cu(0.62) are lower than that for Fe/MgO. The interface anisotropies at the Fe(001)/vacuum and Fe/GaAs(001) interfaces are 0.96 and 1.1 ergs/cm^2, respectively.[19,20] The strength of the uniaxial anisotropy Fe/MgO(001) is comparable to those observed for the Fe/vacuum and Fe/GaAs interfaces.

VI. CONCLUSIONS

We have grown high-quality crystalline tunneling junctions using Fe(001) whiskers and Fe(001) bulk crystals as templates and MgO(001) as a tunneling barrier. RHEED and LEED diffraction patterns indicated that the growth of MgO proceeds in a nearly layer-by-layer mode. Pseudomorphic growth proceeds up to 6 ML. For the deposition of 7 ML or more the strain in the MgO is partially released by a network of misfit dislocations. STM topographic imaging confirmed the two-dimensional nature of the growth and the formation of misfit dislocations. Tunneling spectroscopy was used to show that the MgO films were of high quality and that the MgO tunnel barrier was homogeneous but with a low density of local defects correlated neither to substrate steps nor to misfit dislocations. The measured barrier heights suggest a thickness-dependent band gap in MgO layers. The magnetic properties of Fe films grown on MgO(001) substrates show a large uniaxial anisotropy $K_s=1.1$ ergs/cm^2 with the easy axis perpendicular to the film surface. The BLS spectra show no evidence of exchange coupling between the Fe film and the Fe-whisker substrate.

ACKNOWLEDGMENTS

The authors would like to acknowledge discussions with I. Mertig, C. Schneider, W. Butler, and G. Kirczenow and technical help from K. Myrtle. B.H. acknowledges support by the Alexander von Humboldt Foundation. The SFU group expresses their thanks to the Canadian Granting Agency NSERC for generous financial support.

[1] J.S. Moodera and G. Mathon, J. Magn. Magn. Mater. **200**, 248 (1999).
[2] M. Julliere, Phys. Lett. **54A**, 225 (1975).
[3] W.H. Butler, X.-G. Zhang, T.C. Schulthess, and J. MacClaren, Phys. Rev. B **63**, 054416 (2001).
[4] D. Ullmann, M. Klaua, J. Barthel, and J. Kirschner (unpublished).
[5] L.E. Davis *et al.*, *Handbook of Auger Electron Spectroscopy* (Physical Electronics Industries, Eden Prairie, 1976).
[6] V.E. Henrich and P.A. Cox, *The Surface Science of Metal Oxides* (Cambridge University Press, Cambridge, England, 1999).
[7] P.W. Tasker and D.M. Duffy, Surf. Sci. **137**, 91 (1984).
[8] L.Z. Mezey and J. Giber, Jpn. J. Appl. Phys. **21**, 1569 (1988).
[9] T. Urano and T. Kanaji, J. Phys. Soc. Jpn. **57**, 3403 (1988).
[10] M. Dynna, J.L. Vassent, A. Marty, and B. Gilles, J. Appl. Phys. **80**, 2650 (1996).
[11] If we define a measurable splitting s as the ratio of the distance Δk from a main LEED spot to a satellite spot and the distance $k_\parallel$ of two next main spots, i.e., $s=\Delta k/k_\parallel$, then we can derive from the Ewald construction by simple trigonometry a tilt angle α between the main reciprocal rod and a satellite rod,
$$\alpha=\arctan\{s\cdot k_\parallel/[E/1.9(1+\cos\{\arcsin[k_\parallel(3.81/E)^{1/2}]\})-k_\parallel^2]^{1/2}\},$$
in dependence on the energy E of the electrons. This tilt angle α describes also the s-like sloped regions along the buried dislocation on the MgO surface.
[12] M.C. Gallagher, M.S. Fyfield. J.P. Cowin, and S.A. Joyce, Surf. Sci. **339**, L909 (1995).
[13] E.Y. Tsymbal and D.G. Pettifor, Phys. Rev. B **58**, 432 (1998).
[14] J.L. Vassent, M. Dynna, A. Marty, B. Gilles, and G. Patrak, J. Appl. Phys. **80**, 5727 (1996).
[15] H.L. Meyerheim, R. Popescu, J. Kirschner, N. Jedrecy, M. Sauvage-Simkin, and R. Pinchaux, Phys. Rev. Lett. **87**, 076102 (2001).
[16] W. Wulfhekel, M. Klaua, D. Ullmann, F. Zavaliche, J. Kirschner, R. Urban, T. Monchesky, and B. Heinrich, Appl. Phys. Lett. **78**, 509 (2001).
[17] J. Cochran, J. Magn. Magn. Mater. **169**, 1 (1997).
[18] B. Heinrich, S. Purcell, J. Dutcher, K. Urquhart, J. Cochran, and A. Arrott, Phys. Rev. B **38**, 12 879 (1988).
[19] B. Heinrich and J.F. Cochran, Adv. Phys. **42**, 523 (1993).
[20] T.L. Monchesky, B. Heinrich, R. Urban, K. Myrtle, M. Klaua, and J. Kirschner, Phys. Rev. B **60**, 10 242 (1999).